ECCOMAS Congress 2016
VII European Congress on Computational Methods in Applied Sciences and Engineering
M. Papadrakakis, V. Papadopoulos, G. Stefanou, V. Plevris (eds.)
Crete Island, Greece, 5–10 June 2016

DESIGN OF AXIALLY SYMMETRIC POWER COMBINERS USING SURROGATE BASED OPTIMIZATION

Ryno D. Beyers[1], **Dirk I. L. de Villiers**[1]

[1]University of Stellenbosch
Cnr Banhoek Road & Joubert Street, Stellenbosch, South Africa
e-mail: rdb@sun.ac.za, ddv@sun.ac.za

Keywords: Power Combiners, Coaxial Combiners, Conical Combiners, Circuit Modelling, Surrogate Modelling.

Abstract. *The design and optimization of axially symmetric power combiners usually rely on computationally expensive full-wave simulations. Circuit models are often used to reduce the computational cost, however, full-wave parameter sweeps or optimization are usually still required. Surrogate based optimization utilizing circuit models offers an effective means to reduce the computational cost, since the circuit model can be aligned to the full-wave model, usually resulting in fewer full-wave simulations being required. This paper presents some of the recent advances in using Space Mapping, which is a surrogate based optimization technique, for the design and optimization of axially symmetric power combiners.*

1 INTRODUCTION

Power combiners and dividers have numerous applications and are frequently used in communications and radar systems as part of power amplifier and antenna configurations. Since the introduction of the modern personal computer and electromagnetic analysis software, the design of power combiners/dividers, especially axially symmetric types, has been facilitated by full-wave simulation [1–9]. However, the relatively high computational cost of full-wave simulations limits the amount of the parameter space that can be searched within a reasonable time and cost, thereby possibly limiting the performance that can be attained.

Circuit modelling can be used to various extents to accelerate the design process. For example, circuit modelling can be used for parts of the device with known circuit models, and the rest modelled by full-wave simulation, as is done in [7, 8]. This method reduces the size of the full-wave problem being solved, but it might not be straight-forward to divide the problem into appropriate parts, and full-wave parameter sweeps or optimization are still required to find optimal parameter values. Alternatively, circuit models for the entire device can be constructed, in which case full-wave parameter sweeps or optimization would likely be needed to relate physical dimensions to circuit element values [1, 3, 6]. Empirical data can be used to extract equations for the conversion of dimensions into element values, but these would also require full-wave parameter sweeps in addition to having a fixed and limited range of parameter values where adequate accuracy can be achieved [9].

The use of equivalent circuit models can be exploited, perhaps most effectively, by using Space Mapping [10,11], which is a surrogate based optimization method. By using this method, the optimization burden is moved from the accurate but slow full-wave simulation and placed on the circuit model, which is less accurate, but much faster to evaluate. The use of Space Mapping for the design of conical transmission line power combiners was recently demonstrated in [12], where an optimal design was obtained after only four iterations, requiring only four full-wave simulations. This paper presents guidelines for the Space Mapping based design and optimization of axially symmetric power combiners supporting transverse electromagnetic (TEM) mode propagation. A specific design example of a coaxial line power combiner with an improved fractional bandwidth of $133\ \%$ is presented.

2 EQUIVALENT CIRCUIT MODEL DESCRIPTION

Axially symmetric power combiners generally allow for a large number of devices to be combined with lower losses compared to other power combiner types with the same number of input ports [1, 13]. Non-resonant axially symmetric combiners typically have the added advantage of being able to support TEM modes, and can therefore offer high output port return losses over relatively wide bandwidths when the input ports are excited symmetrically. For these types of combiners the output port is generally referred to as the central port and the input ports as peripheral ports. The design of such a combiner is mostly focussed on obtaining a well-matched transition from the peripheral ports into the combining structure, as well as from the combining structure to the central port. Since ideal transmission lines can be used to model TEM transmission lines, the only non-trivial parts to be modelled are where discontinuities or gradual changes between different transmission line sizes or types occur in the physical structure of the combiner. Examples of some of these discontinuities and gradual changes and how they can be modelled can be found in [1, 5, 8, 14–16]. In most cases, some form of equivalent circuit model can be deduced or found in literature. The requirements of equivalent models used for design or optimization with Space Mapping are that they must be much faster to evaluate than

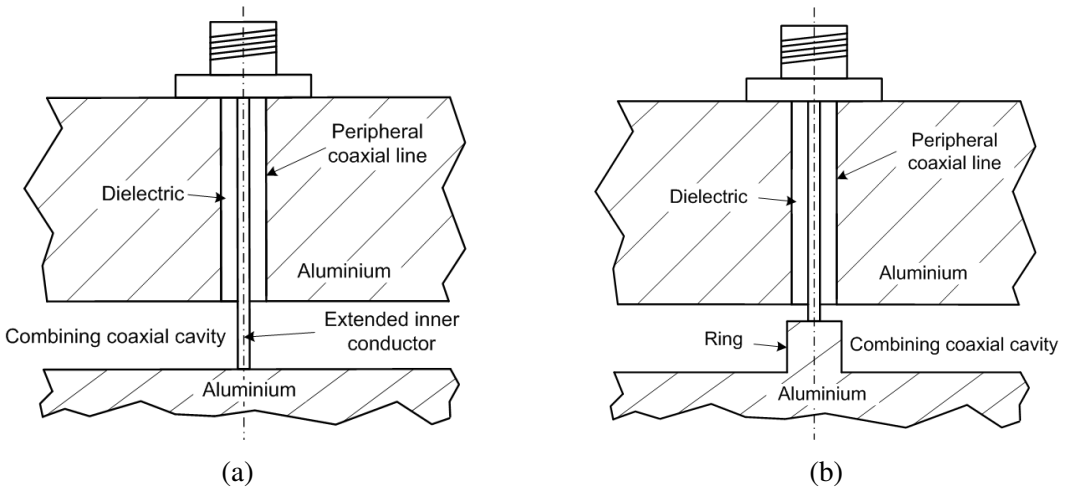

Figure 1: The uncompensated (a) and compensated (b) peripheral coaxial lines used for the input ports of a coaxial power combiner.

the full-wave models and that they can be linked to physical attributes of the structure, similar to how a shunt capacitance is linked to a step discontinuity in a coaxial line. As an example, it will be shown how a circuit model of a coaxial combiner can be obtained. This model will be used for the design example in Section 4.

2.1 Equivalent circuit model of a coaxial combiner

The configuration of the combiner must first be established before it is possible to construct an equivalent circuit model. An appropriate configuration will consist of parts that allow for well-matched transmission, and with equivalent circuit models that are either known or are easy to deduce. It has been demonstrated that the inductance of extended center conductor pins of peripheral coaxial lines (see Fig. 1a), which would normally adversely affect transmission, can be effectively compensated for by using a ring (see Fig. 1b) in the oversized combining coaxial line [6]. The ring-compensated peripheral port transition is therefore an appropriate candidate, since it allows for a well-matched transition, and it is relatively straight-forward to deduce an equivalent circuit model that corresponds well with the physical attributes of the transition, as will be shown in Section 2.1.1. The oversized combining coaxial line can simply be modelled by using ideal transmission lines and shunt capacitances where step discontinuities are introduced for impedance matching purposes. For this design the outer conductor radius will be kept constant and steps will only occur in the inner conductor. The only remaining part of the combiner to be modelled is a transition from the oversized combining coaxial line to the smaller central output port, usually with dimensions corresponding to a standard coaxial connector type. These types of transitions can be physically tapered coaxial lines with a constant impedance [6], or in some cases the impedance can also be tapered, possibly making more efficient use of the overall size of the combiner [3]. For this design, an impedance tapered transition will be used, for which it is straight-forward to deduce an equivalent circuit model, as will be shown in Section 2.1.2. The physical layout of the chosen combiner configuration is shown in Fig. 2, and its equivalent circuit model will now be developed.

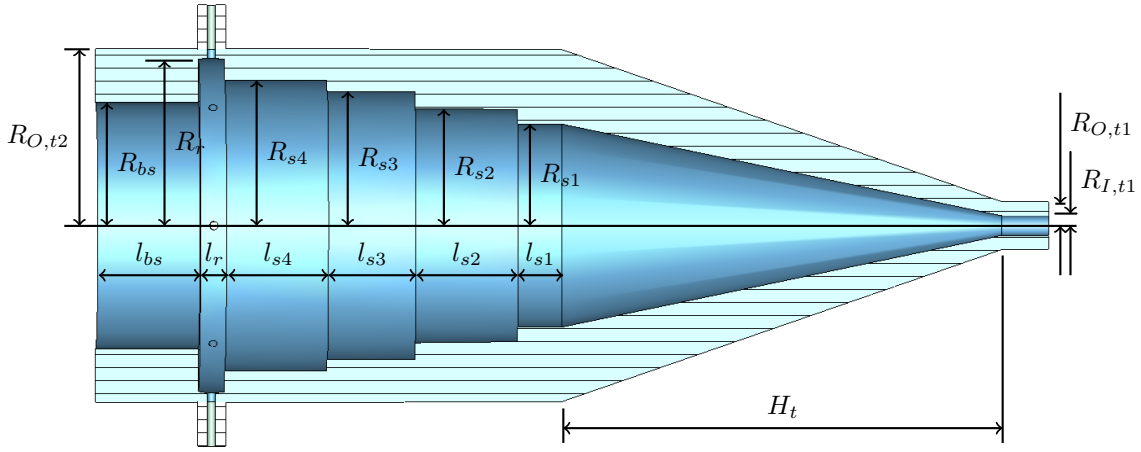

Figure 2: The physical layout of the coaxial combiner with the chosen configuration.

2.1.1 Peripheral coaxial line transition

The ring-compensated peripheral transition proposed in [6] and shown in Fig. 1b shortens the extended center conductor pins of the peripheral coaxial lines, thereby reducing their inductance. It also introduces two step discontinuities, modelled using shunt capacitances, on either side of the peripheral ports inside the oversized combining coaxial line. An additional effect, not taken into account in [6], is that there will be a change in characteristic impedance of the oversized combining coaxial line due to the holes that are made for the outer conductors of the peripheral coaxial lines. However, this perturbance can simply be modelled by using two short transmission lines, one on either side of the peripheral coaxial lines, with appropriately adjusted impedances. The resulting equivalent circuit model is shown in Fig. 3.

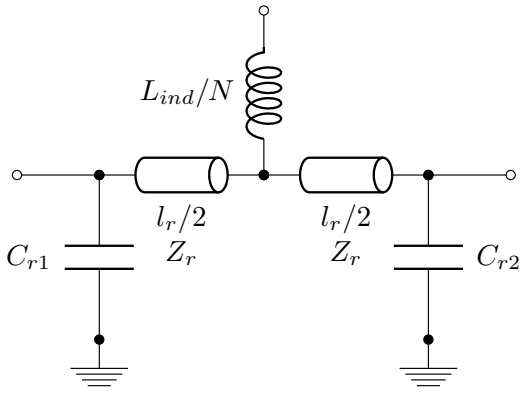

Figure 3: The equivalent circuit model of the peripheral transition.

Note that all circuit element values can be calculated directly from physical dimensions, except for L_{ind} and Z_r, which will be implicit parameters in the Space Mapping based optimization. The length l_r is simply equal to the length of the ring, and the shunt capacitances, C_{r1} and C_{r2}, can be determined by using the information presented in [14]. The values of C_{r1} and C_{r2} can in general be different, since the coaxial line sections on either side of the ring can have different inner conductor radii.

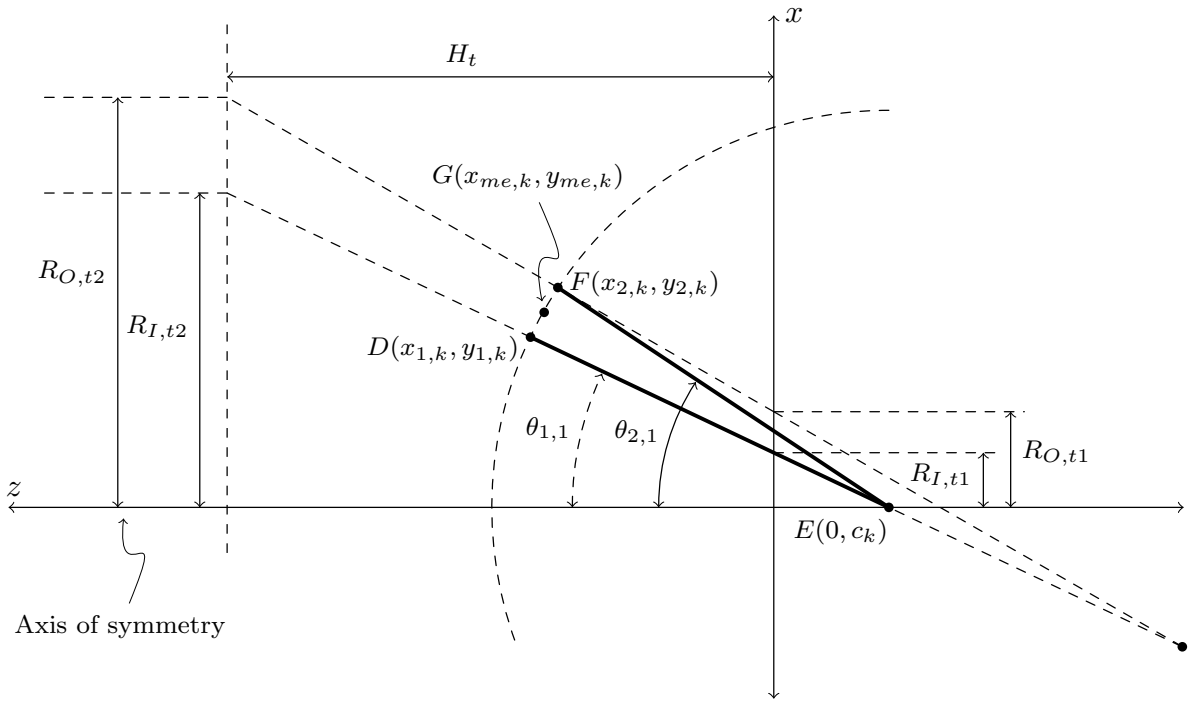

Figure 4: The impedance tapered transition between the central output coaxial line and the oversized combining coaxial line. Note that the figure is rotationally symmetric around the z-axis.

2.1.2 Central impedance tapered coaxial line transition

Even though the central port transition is usually referred to as a tapered coaxial line, it more closely resembles a conical transmission line, and can likely be more accurately modelled as such. A conical transmission line typically consists of two conductors that intersect on the axis of rotational symmetry, forming a transmission line with a constant impedance. An impedance tapered conical line with its conductors tapered at a constant rate (therefore containing no curves, as shown in Fig. 4) would have conductors that do not intersect on the axis of symmetry, and the standard formula for calculating the impedance of a conical transmission line cannot be used. Instead, the tapered transmission line can be approximated by dividing one of the conductors (the lower one, numbered with subscript 1, is chosen here) into K sections and using the simple algorithm described below, with reference to Fig. 4, to determine the impedance and length of each (k-th) section:

1. Draw a line (see line DE) tangential to the conductor from the current position, $D(x_{1,k},y_{1,k})$, to the axis of symmetry, $E(0,c_k)$.

2. Draw a circle centred at $E(0,c_k)$, the intersection of line DE with the axis of symmetry, with a radius equal to the distance from the circle origin to the current position on the conductor, $D(x_{1,k},y_{1,k})$.

3. Find the point of intersection between the circle and the other conductor, $F(x_{2,k},y_{2,k})$.

4. Draw a line (see line FE) from the point of intersection on the second conductor to the circle origin.

5. Use the angles of the two lines, $\theta_{1,k}$ and $\theta_{2,k}$, to calculate the approximate impedance of the current section using the formula for a conical transmission line:

$$Z_k = 60\log\left[\frac{\cot(\theta_{1,k}/2)}{\cot(\theta_{2,k}/2)}\right]. \tag{1}$$

6. Estimate the transmission length of the current section by computing the distance from the mean of the current two points on the conductors, $G(x_{me,k},y_{me,k})$ to the mean of the next two points on the conductors, $(x_{me,k+1},y_{me,k+1})$.

The approximated response of the transition can now be obtained by constructing a circuit with K cascaded ideal transmission lines with impedances and lengths as calculated using the above algorithm.

The accuracy of the circuit model is tested by considering a few different transitions and comparing the circuit model response with full-wave simulations. Fig. 5 shows the approximated impedance profiles of the transitions generated using the parameter values given in Table 1. Transitions 1 and 2 have standard 7/16 connector dimensions for the smaller coaxial line, and Transition 3 has standard N-type dimensions. Fig. 6 shows good agreement between the full-wave and simulated responses of the all the considered transitions.

Transition 1			Transition 2			Transition 3		
Parameter	Value	Units	Parameter	Value	Units	Parameter	Value	Units
$R_{I,t1}$	3.5	mm	$R_{I,t1}$	3.5	mm	$R_{I,t1}$	1.52	mm
$R_{O,t1}$	8	mm	$R_{O,t1}$	8	mm	$R_{O,t1}$	3.5	mm
$R_{I,t2}$	42	mm	$R_{I,t2}$	52	mm	$R_{I,t2}$	20.5	mm
$R_{O,t2}$	60	mm	$R_{O,t2}$	60	mm	$R_{O,t2}$	40	mm
H_t	120	mm	H_t	300	mm	H_t	180	mm

Table 1: Parameter values for the three transitions used to test the equivalent circuit model of the impedance tapered transition.

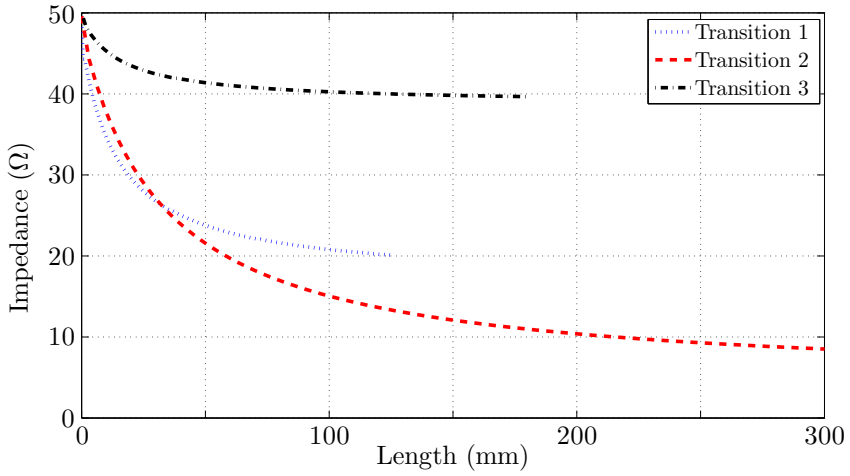

Figure 5: The approximated impedance profiles of the three transitions.

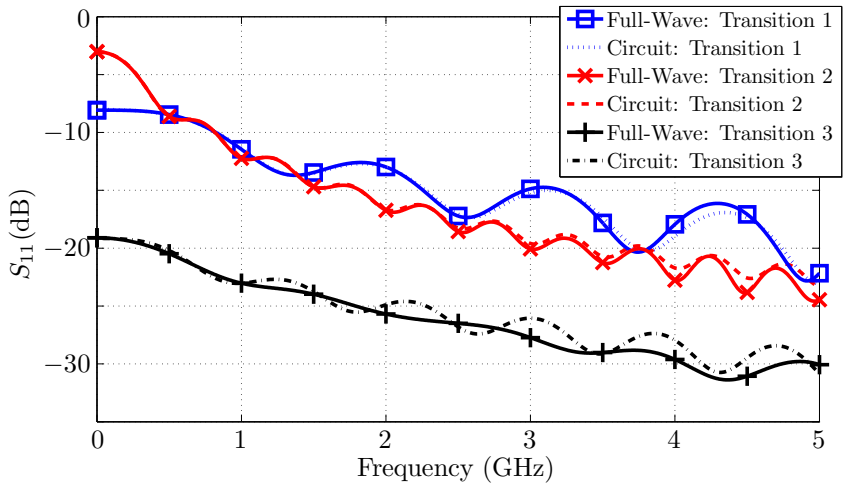

Figure 6: The responses of the circuit model and full-wave simulations.

2.1.3 Complete circuit model

The equivalent circuit models for all parts of the chosen combiner configuration have now been obtained, and can be used to model the entire combiner shown in Fig. 2. The resulting circuit is shown in Fig. 7. The transmission line lengths l_{s1}, l_{s2}, l_{s3}, l_{s4}, l_r, and l_{bs} can be used directly from the physical dimensions of the combiner. The impedances Z_{s1}, Z_{s2}, Z_{s3}, Z_{s4}, and Z_{bs} can be calculated from the inner and outer radii of the respective parts of the combiner using:

$$Z = 60\log\left[\frac{R_{\text{outer}}}{R_{\text{inner}}}\right]. \tag{2}$$

The step capacitances C_{s12}, C_{s23}, and C_{s34} can be calculated using the same method as for C_{r1} and C_{r2} by using the information in [14]. Note that the transmission length of the tapered section, l_t, is not equal to the parameter H_t shown in Figs. 2 and 4. The transmission length l_t and impedance profile Z_t of the central impedance tapered coaxial line transition can be determined from the physical dimensions of the combiner by using the algorithm described in Section 2.1.2. The only parameters with unknown values at this point are Z_r and L_{ind}, which will be implicit parameters in the Space Mapping based optimization.

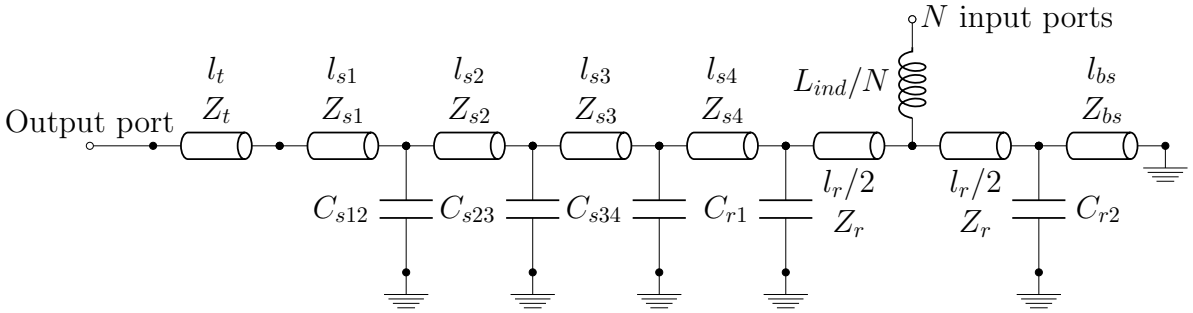

Figure 7: The equivalent circuit model of the entire combiner.

3 OPTIMIZATION STRATEGY

The advantage of using Space Mapping based optimization is that the optimization burden is shifted from the full-wave model (fine model) to the circuit model (coarse model). This is made possible through the alignment of the coarse model with the fine model before being optimized to reach any chosen design goals. The alignment of the coarse model with the fine model can be done using a combination of different methods, however, for this application only multiplicative and additive implicit space mapping (ISM) will be used.

The optimization strategy employed here is essentially the same as in [12]. The goal of the optimization is to obtain the vector of parameter values, $\boldsymbol{x}$, resulting in the lowest cost of the fine model response, $\boldsymbol{R}_f$, given the design objective function, U, and therefore

$$\boldsymbol{x}_f^* = \underset{\boldsymbol{x}}{\operatorname{argmin}}\, U\left(\boldsymbol{R}_f(\boldsymbol{x})\right). \tag{3}$$

Since the main concern when designing axially symmetric combiners that support TEM mode propagation is impedance matching, the response, $\boldsymbol{R}_f$, is usually the central (output) port reflection coefficient, S_{11}, and the objective function, U, defines the desired return loss over the frequency band of interest. Instead of directly optimizing the fine model, ISM produces an approximate solution,

$$\boldsymbol{x}^{(i+1)} = \underset{\boldsymbol{x}}{\operatorname{argmin}}\, U\left(\boldsymbol{R}_s^{(i)}(\boldsymbol{x})\right), \tag{4}$$

which should lead to a solution of (3), where $\boldsymbol{R}_s^{(i)}(\boldsymbol{x})$ is the aligned coarse model (surrogate model) response at the i-th iteration. The surrogate model is constructed by optimizing the implicit parameters, $\boldsymbol{x}_p$, $\left(\boldsymbol{x}_p = [Z_r\ L_{ind}]^T \text{ for the coaxial combiner in Section 2.1}\right)$ to fit the coarse model response onto the fine model response. However, the implicit parameters are not optimized directly: The coefficients $\boldsymbol{G}$ and $\boldsymbol{H}$ are optimized and the implicit parameters calculated using

$$\boldsymbol{x}_p^{(i)}(\boldsymbol{x}) = \boldsymbol{G}\boldsymbol{x} + \boldsymbol{H}, \tag{5}$$

where $\boldsymbol{G}$ is an mxn-matrix, and $\boldsymbol{H}$ is an mx1 matrix, with n the number of design parameters in $\boldsymbol{x}$ and m the number of implicit parameters in $\boldsymbol{x}_p$. The response of the surrogate model can then be obtained using

$$\boldsymbol{R}_s^{(i)}(\boldsymbol{x}) = \boldsymbol{R}_c\left(\boldsymbol{x}, \boldsymbol{x}_p^{(i)}(\boldsymbol{x})\right). \tag{6}$$

As explained in [12], equivalent circuit models for these types of devices are expected to be good representations of their physical structures, and information gained from previous iterations can be used to improve the surrogate models. The previous iterations are therefore taken into account by extracting values for $\boldsymbol{G}$ and $\boldsymbol{H}$ using

$$\boldsymbol{x}_p^{(i)}(\boldsymbol{x}) = \underset{\boldsymbol{G},\boldsymbol{H}}{\operatorname{argmin}} \sum_{k=0}^{i} w_k \left\| \boldsymbol{R}_f\left(\boldsymbol{x}^{(k)}\right) - \boldsymbol{R}_c\left(\boldsymbol{x}^{(k)}, \boldsymbol{x}_p^{(i)}(\boldsymbol{x}^{(k)})\right) \right\|, \tag{7}$$

where $w_k = w_0^{(k+1)}$. Generally $w_0 > 1$ to give the more recent iterations more weight, since it is expected that they will be closer to the optimum point in the parameter space, but $w_0 = 1$ will likely also produce acceptable results.

Each iteration consists of the optimization of the surrogate model, the evaluation of the fine model at the obtained parameter values, and the re-alignment of the coarse model with the fine model, generating a new surrogate model as outlined in (4) - (7). Note that while each iteration may consist of many coarse model evaluations, only a single fine model evaluation is

required. The iterations are repeated until the fine model response reaches the objective or a preset maximum number of iterations are completed. It should be noted that if the parameter extraction is performed using (7), the coarse model evaluation time increases with each iteration due to the increasing number of responses taken into account in (12).

4 DESIGN EXAMPLE: A COAXIAL COMBINER WITH IMPROVED BANDWIDTH

The design of an axially symmetric power combiner using surrogate based optimization will now be illustrated by using the coaxial combiner configuration shown in Fig. 2 and its equivalent circuit model shown in Fig. 7. The circuit model is analyzed using MATLAB, and the fine model evaluations are done using Computer Simulation Technology (CST) Microwave Studio (MWS) [17]. The inner and outer conductor radii of the central output coaxial port, $R_{I,t1}$ and $R_{O,t1}$, are chosen to be the same as the standard $50\ \Omega$ N-type connector, and the outer conductor radius of the oversized combining coaxial line, $R_{O,t2}$ is chosen to be 26 mm. Standard $50\ \Omega$ SMA connector dimensions are chosen for the peripheral feeding coaxial lines, and all the remaining physical dimensions are optimizable parameters. The input parameter vector is thus

$$\boldsymbol{x} = \left[H_t\ R_{s1}\ l_{s1}\ R_{s2}\ l_{s2}\ R_{s3}\ l_{s3}\ R_{s4}\ l_{s4}\ R_r\ l_r\ R_{bs}\ l_{bs}\right]^T, \tag{8}$$

and the implicit parameter vector is

$$\boldsymbol{x}_p = \left[Z_r\ L_{ind}\right]^T. \tag{9}$$

The parameter space is limited to

$$\boldsymbol{x}_{min} = \left[22\ 9\ 5\ 15\ 5\ 20\ 5\ 20\ 5\ 23\ 3\ 13\ 7\right]^T \tag{10}$$

and

$$\boldsymbol{x}_{max} = \left[130\ 20\ 30\ 22\ 30\ 25\ 30\ 25\ 30\ 25.5\ 3.5\ 23\ 25\right]^T, \tag{11}$$

with all values listed in the same order as in (8), and dimensions given in mm. The input parameter vector $\boldsymbol{x}$ contains 13 parameters, and according to (5) the matrix $\boldsymbol{G}$ takes all of these parameters into account in the calculation of $\boldsymbol{x}_p$. This is entirely unnecessary, and as a matter of fact unwanted, since it causes the implicit parameters to be dependent on parameter values they should obviously not be dependent on. For this design, the implicit parameters, Z_r and L_{ind}, are only dependent on the compensation ring radius, R_r. The matrices in (5) are thus reduced to take only R_r into account, resulting in a much more consistent surrogate model being constructed for each iteration. The design objective is to obtain a return loss of greater than 15 dB from 1.3 to 6.5 GHz. The objective function is defined as

$$U(\boldsymbol{R}_f(\boldsymbol{x})) = \frac{1}{i_M - i_m} \sum_{i=i_m}^{i_M} \left|\max\{\boldsymbol{R}_f(\boldsymbol{x}, f_i) - (-15), 0\}\right|, \tag{12}$$

where $\boldsymbol{R}_f(\boldsymbol{x}, f_i)$ is the central port reflection coefficient, S_{11}^{dB}, at frequency f_i, which is at index i in the frequency vector. The indices i_m and i_M correspond to the frequencies 1.3 and 6.5 GHz in f_i, respectively. For the ISM parameter extraction and the surrogate model optimization $w_0 = 1.1$ is chosen, and a global search is first performed using the Population Based Incremental Learning (PBIL) algorithm [18], followed by a local search using the Nelder-Mead simplex search [19]. Given the minimum and maximum values of R_r, some initial values for the implicit parameters are estimated as $Z_r = 4.5\ \Omega$ and $L_{ind} = 2$ nH, using the formula for

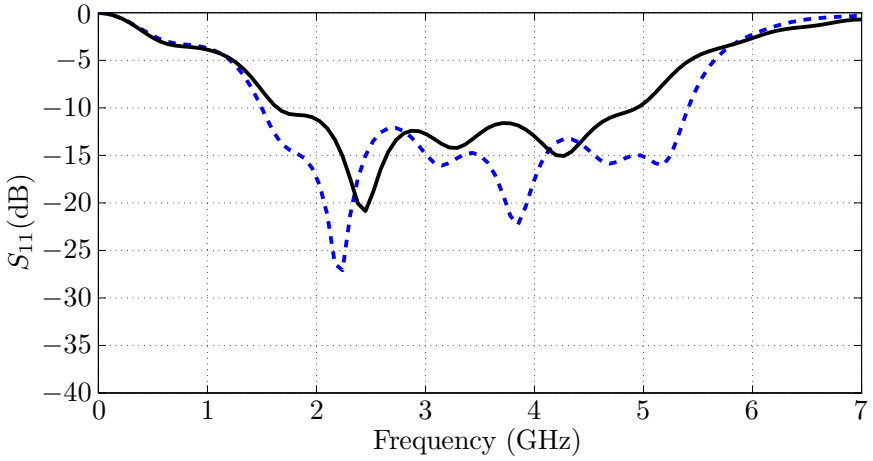

Figure 8: The responses of the surrogate (dashed) and fine (solid) models before alignment.

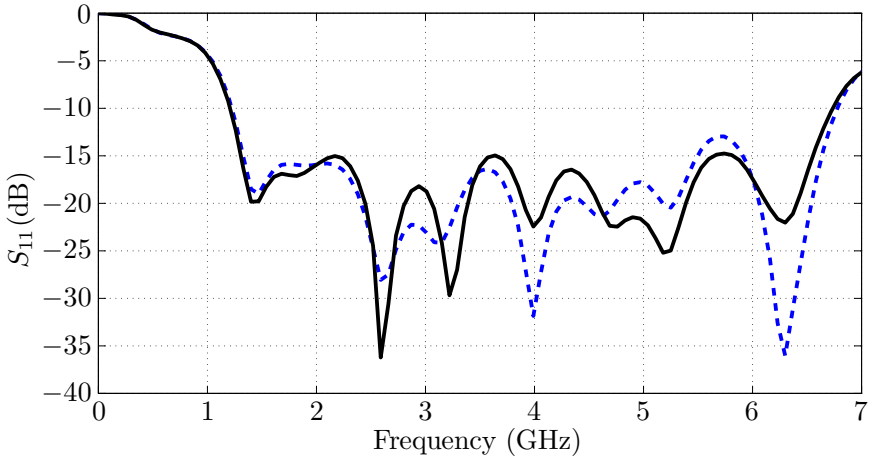

Figure 9: The responses of the surrogate (dashed) and fine (solid) models after 3 iterations.

the impedance of a normal unperturbed coaxial line as given in (2) and the 1 nH per mm rule of thumb. The optimization procedure is executed and the responses of the coarse and fine model are shown in Fig. 8, before the coarse model is aligned. The objective function defined in (12) is shown in Fig. 10 versus iteration number. After 3 iterations the optimization converged and produced the responses shown in Fig. 9, where the fine model response reaches the design objective of a reflection coefficient better than -15 dB over a 133 % bandwidth from 1.3 to 6.5 GHz. The resulting parameter values are listed in Table 2.

5 CONCLUSIONS

This paper presented guidelines for the design and optimization of axially symmetric power combiners. A complete equivalent circuit model of a coaxial combiner was derived using the guidelines. The derived equivalent circuit model was used as a coarse model in a Space Mapping based optimization procedure to design a combiner with improved bandwidth performance. The design objective was to obtain a central port reflection coefficient of better than -15 dB from 1.3 to 6.5 GHz. The optimization procedure converged after 3 iterations and a full-wave simulated

Parameter	Value	Units	Parameter	Value	Units	Parameter	Value	Units
H_t	117.66	mm	l_{s3}	17.34	mm	R_r	23.93	mm
l_{s1}	20.68	mm	R_{s3}	20.02	mm	l_r	3.07	mm
R_{s1}	15.11	mm	l_{s4}	18.59	mm	R_{bs}	14.08	mm
l_{s2}	19.42	mm	R_{s4}	22.38	mm	l_{bs}	9.09	mm
R_{s2}	17.25	mm						

Table 2: Parameter values for the three transitions used to test the equivalent circuit model of the impedance tapered transition.

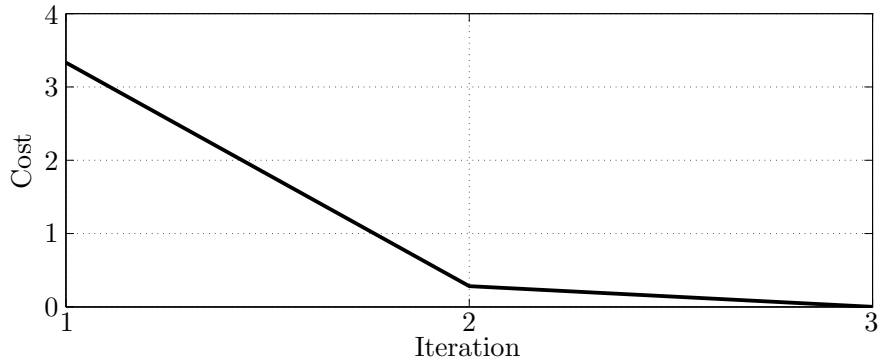

Figure 10: The objective cost after each iteration.

reflection coefficient of better than -15 dB over a 133 % bandwidth from 1.3 to 6.5 GHz was obtained, compared to a measured reflection coefficient of -12 dB over a 112 % bandwidth from 0.52 to 1.86 GHz obtained in [6].

REFERENCES

[1] A. E. Fathy, S. W. Lee, and D. Kalokitis, "A simplified design approach for radial power combiners," *IEEE Transactions on Microwave Theory and Techniques*, vol. 54, no. 1, pp. 247–255, Jan. 2006.

[2] J. M. Denoual, A. Peden, B. Della, and J. P. Fraysse, "16-way radial divider/combiner for solid state power amplifiers in the K-band," in *38th European Microwave Conference Proceedings, (EuMC) 2008*, pp. 345–348, Oct. 2008.

[3] K. Song and Q. Xue, "Planar probe coaxial-waveguide power combiner/divider," *IEEE Transactions on Microwave Theory and Techniques*, vol. 57, no. 11, pp. 2761–2767, Nov. 2009.

[4] X. Shan, Z. Shen, P. Kumaresh, and R. M. Jayasuriya, "A novel 8-way radial power combiner," in *Asia-Pacific Microwave Conference Proceedings, (APMC) 2009*, pp. 2625–2628, Dec. 2009.

[5] Q. Xue, K. Song, and C. H. Chan, "China: power combiners/dividers," *IEEE Microwave Magazine*, vol. 12, no. 3, pp. 96–106, May 2011.

[6] M. Amjadi and E. Jafari, "Design of a broadband eight-way coaxial waveguide power combiner," *IEEE Transactions on Microwave Theory and Techniques*, vol. 60, no. 1, pp. 39–45, Jan. 2012.

[7] D. I. L. de Villiers, P. W. van der Walt, and P. Meyer, "Design of a ten-way conical transmission line power combiner," *IEEE Transactions on Microwave Theory and Techniques*, vol. 55, no. 2, pp. 302–308, Feb. 2007.

[8] D. I. L. de Villiers, P. W. van der Walt, and P. Meyer, "Design of conical transmission line power combiners using tapered line matching sections," *IEEE Transactions on Microwave Theory and Techniques*, vol. 56, no. 6, pp. 1478–1484, Jun. 2008.

[9] R. D. Beyers and D. I. L. de Villiers, "Compact conical-line power combiner design using circuit models," *IEEE Transactions on Microwave Theory and Techniques*, vol. 62, no. 11, pp. 2650–2658, Nov. 2014.

[10] S. Koziel, Q. S. Cheng, and J. W. Bandler, "Space mapping," *IEEE Microwave Magazine*, vol. 9, no. 6, pp. 105–122, Dec. 2008.

[11] S. Koziel, J. W. Bandler, and K. Madsen, "A space-mapping framework for engineering optimization: theory and implementation," *IEEE Transactions on Microwave Theory and Techniques*, vol. 54, no. 10, pp. 3721–3730, Oct. 2006.

[12] D. I. L. de Villiers and R. D. Beyers, "Design of conical transmission line power combiners using space mapping," in *International Conference on Electromagnetics in Advanced Applications, (ICEAA) 2015* , pp. 1437–1440, Sep. 2015.

[13] R. A. York, "Some considerations for optimal efficiency and low noise in large power combiners," *IEEE Transactions on Microwave Theory and Techniques*, vol. 49, no. 8, pp. 1477–1482, Aug. 2001.

[14] P. I. Somlo, "The computation of coaxial line step capacitances," *IEEE Transactions on Microwave Theory and Techniques*, vol. 15, no. 1, pp. 48–53, Jan. 1967.

[15] R. D. Beyers and D. I. L. de Villiers, "Design and analysis of an impedance tapered conical to coaxial transmission line transition," in *44th European Microwave Conference Proceedings, (EuMC) 2014*, pp. 307–310, Oct. 2014.

[16] R. D. Beyers and D. I. L. de Villiers, "Analysis of shorted coaxial peripheral feeding networks for conical line power combiners," in *Asia-Pacific Microwave Conference Proceedings, (APMC) 2013*, pp. 285–287, Nov. 2013.

[17] Computer Simulation Technology AG, Darmstadt, Germany. CST version 2015. [Online]. Available: www.cst.com

[18] S. Baluja, "Population-based incremental learning: A method for integrating genetic search based function optimization and competitive learning," Carnegie Mellon University, Technical Report CMU-CS-94-163, 1994.

[19] J. A. Nelder and R. Mead, "A simplex method for function minimization," *Computer Journal*, vol. 7, pp. 308–313, 1965.